Remote Sensing of Environment 112 (2008) 2898–2913

Contents lists available at ScienceDirect

Remote Sensing of Environment

journal homepage: www.elsevier.com/locate/rse

Coupled retrieval of aerosol optical thickness, columnar water vapor and surface reflectance maps from ENVISAT/MERIS data over land

Luis Guanter [a,*], Luis Gómez-Chova [b], Jose Moreno [c]

[a] GeoForschungsZentrum Potsdam, Remote Sensing Section, Telegrafenberg, D-14473, Potsdam, Germany
[b] Electronic Engineering Department, University of Valencia, Dr Moliner, 50, 46100 Burjassot - Valencia, Spain
[c] Department of Earth Physics and Thermodynamics, University of Valencia, Dr Moliner, 50, 46100 Burjassot - Valencia, Spain

ARTICLE INFO

Article history:
Received 11 December 2007
Received in revised form 7 February 2008
Accepted 7 February 2008

Keywords:
Aerosol optical thickness
Columnar water vapor
Surface reflectance
Atmospheric correction
MERIS
AERONET

ABSTRACT

An algorithm for the derivation of atmospheric parameters and surface reflectance data from MEdium Resolution Imaging Specrometer Instrument (MERIS) on board ENVIronmental SATellite (ENVISAT) images has been developed. Geo-rectified aerosol optical thickness (AOT), columnar water vapor (CWV) and spectral surface reflectance maps are generated from MERIS Level-1b data over land. The algorithm has been implemented so that AOT, CWV and reflectance products are provided on an operational manner, making no use of ancillary parameters apart from those attached to MERIS products. For this reason, it has been named *Self-Contained Atmospheric Parameters Estimation from MERIS data* (SCAPE-M). The fundamental basis of the algorithm and applicable error figures are presented in the first part of this paper. In particular, errors of ±0.03, ±4% and ±8% have been estimated for AOT, CWV and surface reflectance retrievals, respectively, by means of a sensitivity analysis based on a synthetic data set simulated under a usual MERIS scene configuration over land targets. The assumption of a fixed aerosol model, the coarse spatial resolution of the AOT product and the neglection of surface reflectance directional effects were also identified as limitations of SCAPE-M. Validation results are detailed in the second part of the paper. Comparison of SCAPE-M AOT retrievals with data from AErosol RObotic NETwork (AERONET) stations showed an average Root Mean Square Error (RMSE) of 0.05, and an average correlation coefficient R^2 of about 0.7–0.8. R^2 values grew up to more than 0.9 in the case of CWV after comparison with the same stations. A good correlation is also found with the MERIS Level-2 ESA CWV product. Retrieved surface reflectance maps have been successfully compared with reflectance data derived from the Compact High Resolution Imaging Spectrometer (CHRIS) on board the PRoject for On-Board Autonomy (PROBA) in the first place. Reflectance retrievals have also been compared with reflectance data derived from MERIS images by the Bremen AErosol Retrieval (BAER) method. A good correlation in the red and near-infrared bands was found, although a considerably higher proportion of pixels was successfully processed by SCAPE-M.

1. Introduction

Many advances in instrumental design and processing algorithms for Earth Observation purposes have been achieved in the last decade. Those advances have enabled the launch of the ENVIronmental SATellite (ENVISAT) mission by the European Space Agency (ESA) on March 2002. ENVISAT is currently the ESA core mission for Earth Observation. Different instruments were placed on board ENVISAT. The MEdium Resolution Imaging Specrometer Instrument (MERIS) (Rast et al., 1999) is one of them. A large volume of ENVISAT/MERIS data are now available on-line. ESA Earth Observation data policy depends on the use of the data. Users with an on-going project can access to MERIS products (Amans & Laur, 2007)[1].

Even though MERIS was primarily dedicated to ocean color observations, it broadened its scope of objectives to atmospheric and surface studies. This is enabled by MERIS spectral configuration, which provides a good characterization of cloud features, particle scattering, water vapor absorption and land parameters at a medium resolution spatial scale. MERIS is a programmable, medium-spectral resolution, imaging spectrometer operating in the visible and near-infrared (VNIR) reflective spectral range. It is designed so that high radiometric (1 to 5%) and spectrometric (1 nm) performance are achieved. MERIS 68.5° field of view (FOV) around nadir covers a swath width of 1150 km at a nominal altitude of 800 km. It allows global coverage of the Earth in 3 days. Fifteen spectral bands can be selected by ground command, although a fixed set of bands was recommended by the MERIS Science Advisory Group. These are centered at 412.5, 442.5, 490, 510, 560, 620, 665, 681.25, 708.75, 753.75, 760.625, 778.75, 865, 890 and 900 nm, respectively, within the ±1 nm uncertainty associated to spectral calibration. Typical bandwidths are about 10 nm. Pixel size is about 300 m for full spatial resolution (FR) data and about 1.2 km for reduced

* Corresponding author.
E-mail address: luisguan@gfz-potsdam.de (L. Guanter).
[1] http://earth.esa.int/dataproducts/accessingeodata/howtoaccess.html.

0034-4257/$ – see front matter © 2008 Elsevier Inc. All rights reserved.
doi:10.1016/j.rse.2008.02.001

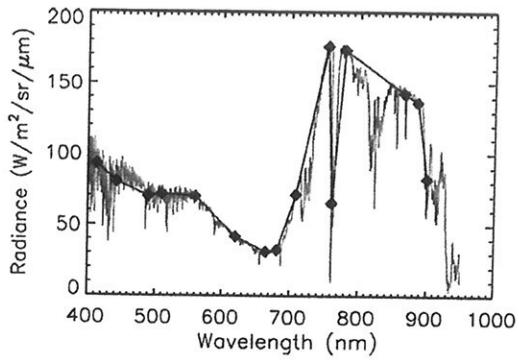

Fig. 1. Simulated green vegetation radiance spectrum at the Top-of-Atmosphere. Diamonds mark the resampling to MERIS band configuration.

spatial resolution (RR) data. A simulated green vegetation radiance spectrum resampled to MERIS band configuration is plotted in Fig. 1. The good sampling of the visible region of the spectrum, typically used for the retrieval of aerosol loading over land targets, and the registration of the oxygen-A absorption (band 11) and the left wing of the 940 nm water vapor absorption (band 15) can be stated.

Most of the algorithms for the exploitation of optical remote sensing data use surface reflectance as a starting point. The conversion from Top-Of-Atmosphere (TOA) radiance to surface reflectance, so-called atmospheric correction, must correct for the distortion caused by the interaction between solar radiation and atmospheric components. The atmospheric parameters with the highest optical activity in the spectral range covered by the sensor must be estimated prior to the derivation of surface reflectance. Clouds, ozone, aerosol loading and water vapor are the most active atmospheric components in the VNIR range covered by MERIS. Cloudy pixels are masked out for land surface studies, and default climatology values are usually applied for the ozone column content due to its low temporal and spatial variability. For aerosols and water vapor the situation is different, as they vary strongly in small spatial and temporal scales. Coincidence of this atmospheric information with the image to be processed is needed. The most efficient way to achieve this coincidence is the retrieval of the atmospheric parameters from the image itself. The resulting aerosol and water vapor data can then be used not only for the retrieval of surface reflectance, but also as input for atmospheric characterization studies.

Methods for the retrieval of aerosol optical thickness (AOT), columnar water vapor (CWV) and surface reflectance were implemented in the MERIS Ground Segment (GS) to provide users with those parameters as part of the MERIS Level-2 (L2) products. The atmospheric correction algorithm implemented in the GS (Santer et al., 1999) consists of three separate steps, the estimation and correction for aerosol effects being one of them. In turn, the MERIS L2 CWV product (Bennartz & Fischer, 2001) generated by the GS is separated from atmospheric correction. Although the consistency of the CWV product over land has been thoroughly tested and validated (e.g. Li et al., 2003; Ciotti et al., 2003), some controversy has been traditionally associated to the MERIS aerosol and subsequent reflectance products. The main problem was the low coverage of the aerosol product over land, due to the use of the dense dark vegetation (DDV) concept (Kaufman & Sendra, 1988). This results in a poor sampling due to aerosol loading is only estimated over those pixels covered by very dark vegetation, which are seldom available in many areas of the planet. As a consequence, the MERIS L2 reflectance product was delivered without aerosol correction. Although the surface model for the aerosol retrieval algorithm in the GS has been recently reviewed for a broader application range (Santer et al., 2007), the Bremen AErosol Retrieval algorithm (BAER) (von Hoyningen-Huene et al., 2003, 2006) was implemented in the Basic ERS & Envisat (A)ATSR and MERIS (BEAM) Toolbox (Fomferra & Brockmann, 2005) in order to convert from L2 "Top-Of-Aerosols" reflectance to actual surface reflectance. It is not available for the atmospheric correction of MERIS Level-1b (L1b) data. Some of the low spatial sampling in aerosol retrieval was solved by BAER, but no continuous aerosol and surface maps from MERIS data over land are yet available. Another method for the aerosol retrieval from MERIS data is presented in Béal et al. (2007), but no information about the spatial sampling and performance for surface reflectance retrieval has been found. Overall, there is a number of atmospheric correction methods for MERIS data over land, mostly focusing on the retrieval of aerosol information, without considering other factors such as water vapor residual absorption or elevation and topographic effects.

The method presented in this paper is intended to support the renewed interest in MERIS data for atmospheric and land studies, as well as to provide the MERIS community with a new consistent tool for the processing of MERIS L1b data. In particular, geo-rectified maps of aerosol optical thickness, columnar water vapor and surface reflectance are automatically generated. This autonomous working is summarized in the name chosen for the corresponding computer code, *Self-Contained Atmospheric Parameters Estimation from MERIS data* (SCAPE-M). An earlier version of SCAPE-M was already described in Guanter et al. (2007) (submitted for publication in January 2005, accepted in February 2006), but some of the algorithm steps were uncompleted, nor error budgets were estimated for the different products, and little validation was carried out. The final operational version of SCAPE-M is presented in this paper. The fundamental basis of the algorithm is described in Section 2; a sensitivity analysis to estimate approximate error figures associated to the different retrievals will be exposed in Section 3. The validation of SCAPE-M retrievals by comparison with AErosol RObotic NETwork (AERONET) (Holben et al., 1998) measurements and other data sources is presented in Section 4. Finally, a summary of the most important findings is reported in Section 5.

2. Methodology

2.1. Radiative transfer calculations

The retrieval of atmospheric constituents and surface reflectance involves modeling the radiative transfer across the atmosphere. A simple but accurate formulation of the TOA signal in terms of surface reflectance and atmospheric optical parameters is necessary. Since MERIS does not provide multiangular measurements, as long as multitemporal series of images are not available, the usual Lambertian approach (Nicodemus et al., 1977) is assumed for surface reflectance. This leads to the well-known equation:

$$L_{TOA} = L_0 + \frac{1}{\pi}\frac{\rho_s(E_{dir}\mu_{il} + E_{dif})T_{\uparrow}}{1 - S\rho_s} \quad (1)$$

where L_{TOA} is the TOA radiance measured by the sensor; L_0 is the atmospheric path radiance; μ_{il} is the cosine of the illumination zenith angle, measured between the solar ray and the surface normal; $E_{dir}\mu_{il}$ and E_{dif} are the direct and diffuse fluxes arriving at the surface, respectively; S is the atmospheric spherical albedo, reflectance of the atmosphere for isotropic light entering it from the surface; $T_{\uparrow}$ is the total atmospheric transmittance (for diffuse plus direct radiation) in the observation direction, and ρ_s is the surface reflectance.

MODTRAN4 atmospheric radiative transfer code (Berk et al., 2003) was used for the generation of a Look-Up Table (LUT) which provides the atmospheric parameters from multidimensional linear interpolation. MODTRAN4 has been selected for its accurate parametrization of both scattering and absorption atmospheric processes, as imposed by an algorithm dealing with simultaneous aerosol and water vapor retrieval. It depends on 6 free input parameters: View Zenith Angle (VZA), Solar Zenith Angle (SZA), Relative Azimuth Angle (RAA), surface elevation (ELEV) above sea level (ASL), horizontal visibility (VIS) and columnar water vapor (CWV). Horizontal visibility is the natural input parameter in MODTRAN4 for aerosol loading. The conversion from VIS to AOT at the reference wavelength of 550 nm is performed

Table 1
Breakpoint positions in the LUT for the 6 input variables

	#1	#2	#3	#4	#5	#6	#7
VZA (°)	0	9	18	27	36	45	–
SZA (°)	0	10	20	35	50	65	–
RAA (°)	0	25	50	85	120	155	180
ELEV (km)	0	0.7	2.5	–	–	–	–
VIS (km)	10	15	23	35	60	100	180
CWV (g cm^{-2})	0.3	1	1.5	2	2.7	5	–

afterwards, taking into account elevation effects on a per-pixel basis. The original MODTRAN4 code was modified so that the atmospheric optical parameters needed for the atmospheric correction in Eq. (1) were provided as output, as they are not in the original MODTRAN4 code (Guanter et al., in press). The optimum breakpoint positions for the 6 input parameters are presented in Table 1.

The number of breakpoints describing each dimension in the LUT was selected as a trade-off between sufficient sampling and LUT size. For this purpose, radiative transfer simulations provided the dependencies of physical magnitudes on the 6 free parameters. A number from 3 to 7 provided a sufficient sampling of the parameter space without leading to unaffordable computation times or LUT size. For the selection of breakpoint positions, their influence on scattering and absorption processes was analyzed. Atmospheric path radiance at the MERIS shortest wavelength (412.5 nm) was selected to describe scattering, while the total irradiance (Eg) ratio between pairs of absorption/reference bands were used as a proxy to atmospheric absorption. Breakpoints positions were selected so that the maximum parameter variation rates were properly sampled. Example cases for SZA, RAA and ELEV are shown in Fig. 2. The varying number of breakpoints needed to describe the dependencies of absorption and scattering processes with the different parameters can be observed. Further tests have been performed on these and other parameters prior to the LUT definition.

The use of the LUT for the calculation of atmospheric optical parameters enables accounting for pixel-to-pixel variations caused by changes in the surface elevation. The Global Earth Topography And Sea Surface Elevation at 30 arc sec resolution (GETASSE30) Digital Elevation Model (DEM) supplied with the BEAM Toolbox is automatically co-registered to MERIS images to provide elevation data.

2.2. Masking non-land pixels

The initial step of the atmospheric correction algorithm is masking out all but cloud-free land pixels. Pixels with surface elevation higher than 2500 m, which is the upper limit for elevation in the atmospheric LUT, pixels labelled as Invalid in MERIS L1b flags, and pixels with self-shadowing effects (those which are not directly illuminated because of topographic interference) are also discarded.

The most difficult contribution to be separated from land pixels is that coming from clouds over continental areas. A cloud mask to eliminate pixels totally or partially affected by clouds must be generated prior to the estimation of aerosol loading and water vapor content. Utilizing the Cloud Probability Processor implemented in the BEAM Toolbox (Fomferra & Brockmann, 2005) as a plug-in in the atmospheric correction software was considered in the first place. It calculates the cloud probability (0–100%) for every pixel. However, similar cloud probabilities were found in cloudy pixels and in bright cloud-free bare soils. Then, the large data set of images acquired over the Iberian Peninsula (which was one of the main data sources to test the algorithm) could hardly be processed with that method, as an important contribution from bright soils is found.

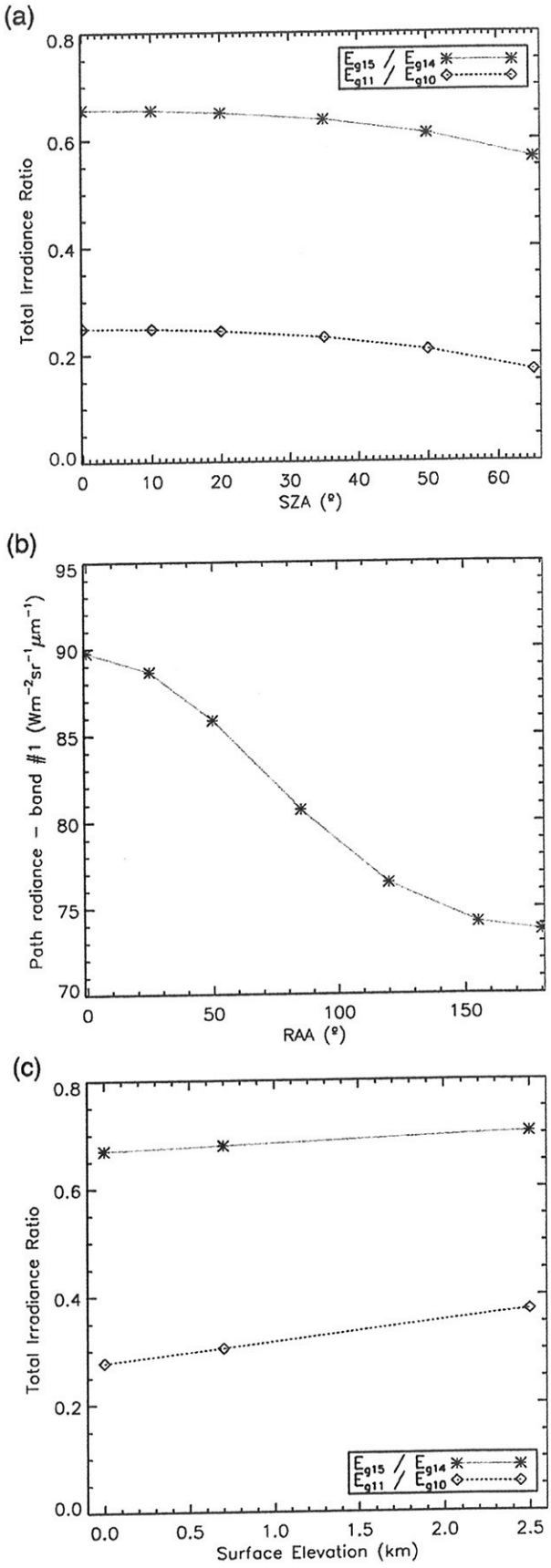

Fig. 2. Dependence of atmospheric absorption (irradiance ratio between pairs of absorption/reference bands) and scattering (path radiance at 412.5 nm) processes on SZA, RAA and ELEV parameters.

Thus, a simpler but more robust cloud masking method based on static thresholds over TOA reflectance and TOA reflectance spectral slope has been designed. In its current status, two sets of thresholds were empirically selected. The first of them, cloud mask #1, is very restrictive in order to ensure AOT retrieval is only performed over cloud-free and non-bright pixels. This is done because even the thinnest cloud may affect considerably aerosol retrievals, leading to a large AOT overestimation. The second set of thresholds, cloud mask #2, is designed to discriminate pixels in which the contamination by clouds is ensured. It is intended to be applied in the CWV and surface reflectance retrieval, in which thin clouds do not have such a large impact. The two threshold sets are:

- cloud mask #1: $\rho^{av}_{TOA}>0.27$, $\rho^{1}_{TOA}>0.2$, $\rho^{1}_{TOA}>\rho^{8}_{TOA}$
- cloud mask #2: $\rho^{av}_{TOA}>0.3$, $\rho^{1}_{TOA}>0.23$, $\rho^{1}_{TOA}>\rho^{9}_{TOA}$

where ρ^{av}_{TOA} is the average TOA reflectance at visible wavelengths, calculated as the average reflectance in channels 1 to 8 (412.4–681.3 nm), and ρ^{i}_{TOA} refers to the TOA reflectance in MERIS band i.

The cloud masking method performance is illustrated in Fig. 3. The two threshold sets were applied to a MERIS FR image on last 15 May 2003 over Toulouse, France. The subset shown in Fig. 3(a) corresponds to an area of about 120×120 km where thick and thin clouds were present. Fig. 3(b) is derived with the threshold set labelled as cloud mask #1, while Fig. 3(c) results from cloud mask #2. It can be stated that the thickest clouds are well detected in both cases, but it does not happen the same for the thinnest ones, that are only masked by cloud mask #1. The adaptation of a more sophisticated method based on classification using different absorption features as well as brightness and spectral slope criteria (Gómez-Chova et al., 2007) is foreseen for future versions of SCAPE-M.

Even though SCAPE-M is intended to work over land surfaces, inland water bodies up to 400 km^2 and coastal pixels separated up to 10 km from the coast line are also processed, as the atmospheric parameters derived from land pixels can be extended to those areas. The largest water bodies are removed by discarding all the closed regions labelled as water with an area higher than 400 km^2, but keeping the pixels in a 10 km distance from the coast line provided by the MERIS Level-1b Coastline flag. The Land/Sea flag cannot be used for the classification of inland water bodies because some of them are missing in the existing data base. This ability of SCAPE-M to process inland and coastal water pixels is a further advantage of SCAPE-M with respect to existing land-focused atmospheric correction algorithms like BAER.

2.3. Topographic effects

The area covered by MERIS scenes is usually from 350 to 1100 km, depending on the scene type. This means that rugged surfaces usually appear within the images. Techniques aimed to accounting for topographic effects in remote sensing images have been developed by a number of authors. Most of them (Colby, 1991; Franklin & Giles, 1995; Riaño et al., 2003) perform a simple topographic correction prior to the atmospheric correction which is based on weighting the measured radiance by the cosine of the illumination angle as measured from the surface normal vector. However, the dependence of the global flux at the surface on varying terrain slopes and orientations is related to the atmospheric state, as the ratio between direct and diffuse terms is weighted by the atmospheric transmittance. This fact suggests atmospheric correction to be coupled to the correction of topographic effects (Richter, 1997). The effect of changing terrain slope and orientation on the direct flux is taken into account in SCAPE-M by applying a standard cosine correction, whereas the Hay's model (Hay, 1979) is used for the anisotropic distribution of the diffuse irradiance. The surface normal vector is calculated on a per-pixel basis by means of the inversion of the plane equation $ax+by+cz+d=0$ against the nine elevation points in a

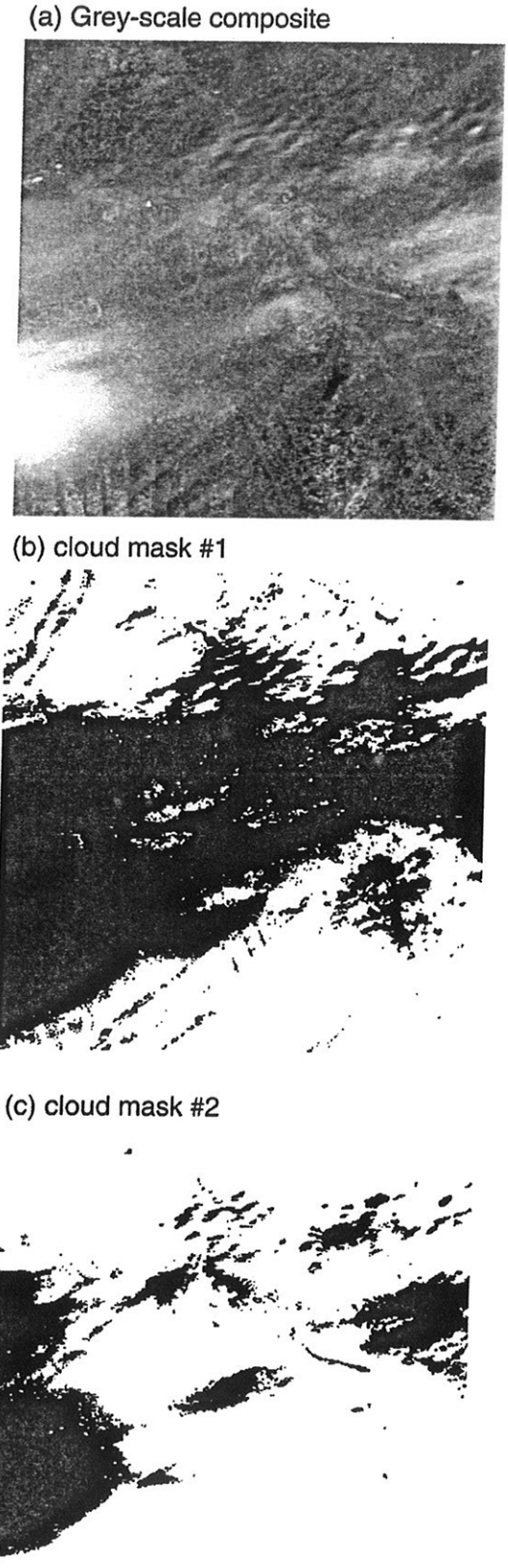

Fig. 3. Example of the cloud masking technique performance. The grey composite in (a) corresponds to a subset extracted from a MERIS FR image acquired over Toulouse, France (latitude=43.6°N, longitude=1.4°W, mean elevation=150 m) on 15 May 2003. Threshold sets cloud mask #1 and cloud mask #2 lead to (b) and (c), respectively.

3×3 pixels square grid around a given pixel. The cosine of the actual illumination angle μ_{il} is calculated as the scalar product between the surface normal vector and the target-to-sun vector.

An example of μ_{il} variations within a MERIS FR image acquired over the Iberian Peninsula (center coordinates about latitude=39.5°N, longitude=4.0°W) on 26 July 2003 is displayed in Fig. 4. The derived μ_{il} image is compared with the DEM of the same area. Sun position at the image center is SZA=27.2° and SAA=131.7° (μ_s=cos(SZA)=0.89, South–East illumination). It can be observed that illumination angles are highly variable in rugged surfaces, as illuminated and shadowed areas can be easily identified. The negative gradient in the illumination from South–East to North–West due to μ_s variations across the images can also be detected. Most of the actual illumination angles vary from 0° to 40° in the images, while SZA is between 23.4° and 30.9°. This leads to changes in the direct irradiance arriving at the surface of about 10%, which could generate errors in the retrieved reflectance higher than those due to a mis-estimation of the atmospheric constituents or the assumption of a Lambertian surface in many combinations of geometrical configurations and atmospheric states.

2.4. Retrieval of AOT

Aerosol extinction is parameterized by visibility (equivalent to AOT at 550 nm) and the rural aerosol model (Shettle & Fenn, 1979). The first one provides the total aerosol loading, while the rural model specifies the spectral slope of aerosol extinction. Concerning aerosol type, early versions of SCAPE-M tried to derive information about the aerosol model, but it was concluded that there is not enough information on MERIS data over land (that is, relatively bright targets at the NIR wavelengths, one single view angle and a reduced spectral range from 400–900 nm) to achieve a reliable estimation of the aerosol model. The difficulties to estimate the aerosol model from MERIS data were also reported in Santer et al. (2005) and Ramon and Santer (2005). The same is true for Moderate Resolution Imaging Spectroradiometer (MODIS) (Remer et al., 2005) and Advanced Along-Track Scanning Radiometer (AATSR) (Grey et al., 2006b) data. The validity of fixing the aerosol model to rural aerosols for a large proportion of cases is probed in Béal et al. (2007).

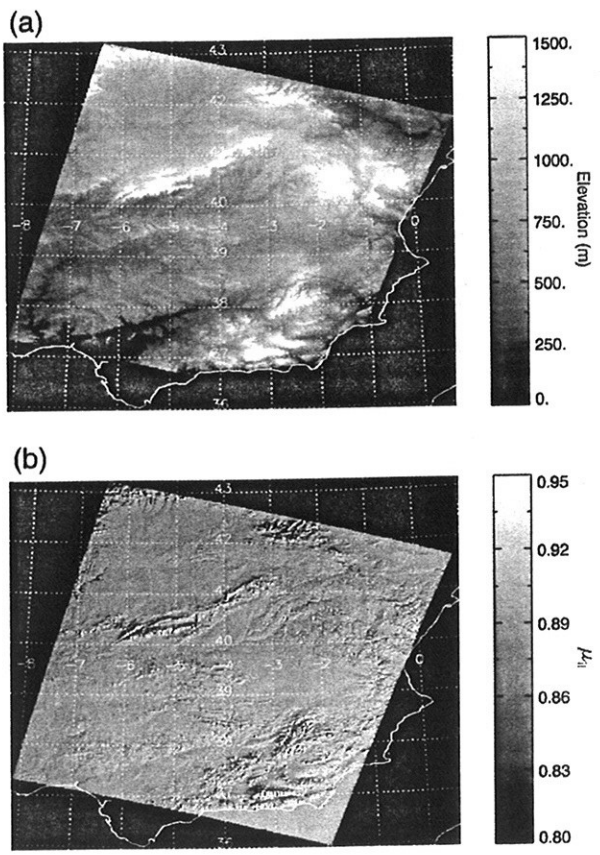

Fig. 4. Actual illumination angles within a MERIS FR image acquired over the Iberian Peninsula. Up (a), elevation of the area provided by GETASSE30 DEM. Down (b), μ_{il} image calculated from the DEM in (a) and the corresponding SZA image.

Aerosol retrieval in SCAPE-M is based on the assumption that the atmospheric state is invariant inside 30 km×30 km cells. Aerosol loading is estimated sequentially from all the 30 km×30 km cells in the image by means of a sliding window with given mean VZA, SZA, RAA and surface elevation. The 30 km size is chosen as a trade-off between the largest area in which the atmosphere can be considered constant and the smallest one providing enough variability in the surface. Even though this gridding leads to the degradation of the aerosol product spatial resolution, it provides important advantages in terms of spatial sampling and retrieval robustness. The use of spatial cells for aerosol remote sensing is also used by e.g. MODIS (Kaufman et al., 1997; Remer et al., 2005) and AATSR (Grey et al., 2006a,b) aerosol retrieval algorithms.

The first step is masking out all the pixels affected by cloud contamination. Making use of cloud mask #2, those pixels which are sure to be cloudy are removed. Visibility from a given cell is calculated as long as it contains more than 35% of cloud-free pixels. If the percentage of cloud-free pixels is lower than 35% it is assumed that the cell is too contaminated by clouds for a reliable aerosol retrieval. The lowest radiance value in each spectral band within the cell is found then. The resulting spectrum is employed somehow similarly to a dark target. It provides the highest limit for the aerosol content: an iterative procedure looks for the visibility value leading to the atmospheric path radiance which is closest to the radiance in the dark spectrum, not allowing path radiance to be higher than the dark spectrum in any of the visible bands (from 412 to 681 nm). The lower the radiance in the dark spectrum is, the closer the estimated visibility value will be to the real value. If no spectrum with relatively dark values is found, the retrieved aerosol loading will overestimate the real conditions. To avoid this situation, a lower limit of 45 km (AOT at 550 nm about 0.2) is arbitrarily chosen: if the estimated visibility is lower than 45 km, the dark pixel estimation for that cell is discarded.

The next step is refining that initial visibility estimation with a more sophisticated method involving the inversion of TOA radiances in combinations of green vegetation and bare soil pixels. This is performed only over those pixels which are classified as land pixels by cloud mask #1. The visibility in each of the cells is then retrieved from 5 pixels with high spectral contrast inside this window, by means of a multiparameter inversion of the TOA spectral radiances in those pixels. To provide an estimation of the surface reflectance each of the 5 reference pixels is represented by a linear combination of two vegetation and soil spectra, which act as endmembers. The proportions of vegetation and soil are allowed to be larger than 100%, covering those cases in which the surface reflectance is brighter than the endmembers. The constraint is that the generated surface reflectance must be in the range [0,1]. The ten abundance coefficients (2 for each of the 5 pixels) are free parameters in the inversion, as well as the aerosol loading. The resulting 11-D inversion is performed by the Powell Minimization Method (Press et al., 1986). It must be remarked that the vegetation and bare soil endmembers are not real endmembers characterizing every single scene, but they are only used to represent the average surface reflectance contribution by means of its linear combination. Thus, there is no need for the retrieval of endmembers from the image, but it is enough if the a priori selected spectra can be combined to reproduce the actual spectral shape of the reference pixels. A similar idea using linear combinations of endmembers to be inverted inside an AOT retrieval scheme, although on a per-pixel basis, was also proposed by von Hoyningen-Huene et al. (2003, 2006).

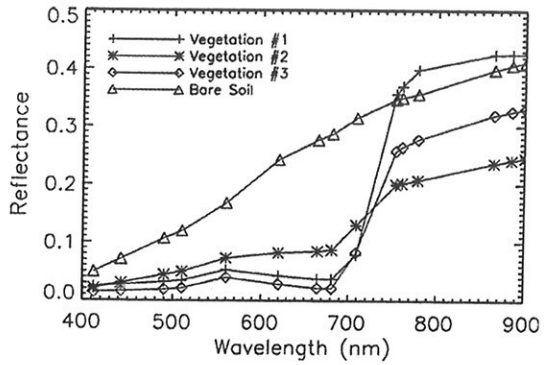

Fig. 5. Vegetation and bare soil reflectance spectra used as endmembers in the aerosol retrieval module. The vegetation spectra correspond to a green vegetation crop (Vegetation #1), a typical forest spectrum (Vegetation #2) and a dark vegetation target (Vegetation #3).

The selection of 5 as the number of pixels to serve as reference for AOT retrieval comes from a balance between the computation burden and the representative sampling in the 30×30 km^2 window. The 5 reference pixels must have as much spectral contrast as possible (ranging from pixels with high vegetation content to high bare soil content). The reason is that this contrast in the surface, while assuming a constant atmosphere above, is used in the discrimination of the radiative transfer contribution of surface and atmosphere to the TOA signal. The DEM projected onto the image is used to ensure that the selected pixels do not present variations larger than ±20% in the surface elevation and ±10% in the illumination angle μ_{li}. In both cases, larger variations would add errors to the retrievals. Variations in the surface elevation might cause differences in the Rayleigh contribution, while changes in the illumination angle would modify the amount of radiation in the system.

In order to minimize possible biases due to a bad representation of the actual surface reflectance by endmember combinations, three different vegetation spectra are combined with one bare soil spectrum to simulate each reference pixel. Those three vegetation spectra, plotted in Fig. 5, correspond to a green vegetation crop, a typical forest spectrum and a dark vegetation target. The aerosol loading is calculated independently for each of the three pairs of vegetation and soil endmembers. The AOT value leading to the minimum value of the merit function driving the inversion is selected for the cell. The reason for having 3 vegetation spectra accounting for different vegetation types and only one for bare soil is that vegetation is considered to have a wider range of spectral patterns than bare soils. These are considered to be less variable in spectral terms, while may have important variations in brightness, which are already modulated by the abundance factor.

After visibility estimations are derived for each of the cells in which the retrieval is successful, the resulting mosaic is smoothed in order to reproduce the smooth variations expected in the atmospheric distribution. Blank cells (namely those with a proportion of land pixels smaller than 35%) are filled by means of interpolation with the surrounding ones. If there were no neighbors with data to perform the interpolation for a given cell, visibility would be set to the mean value calculated from all the occupied cells. A cubic convolution interpolation method is used to convert from cell to pixel scale. The final visibility map is generated after masking the per-pixel visibility image with cloud mask #2. The last step is the conversion from horizontal visibility to AOT at 550 nm by means of bilinear interpolations providing AOT as a function of visibility and surface elevation. The most important steps for the derivation of AOT maps are depicted in Fig. 6.

2.5. Retrieval of CWV

The water vapor retrieval module in SCAPE-M is based on a differential method which evaluates the radiances inside and outside the water vapor absorption feature registered in MERIS band 15. It is run after the aerosol estimation in order to eliminate errors in CWV which would arise if the aerosol loading is not known (Bennartz & Fischer, 2001; Chylek et al., 2003). It can be stated in Fig. 1 that MERIS band 14 (centered at 890 nm) is free from water vapor absorption, while band 15 (centered at 900 nm) is affected by one of the wings of the water vapor absorption feature centered at 940 nm.

The basis of the method is to invert the ratio R of the radiance at MERIS band 15 to the one at 14, CWV being the only free parameter in the inversion. With this purpose, a simulated ratio R^{SIM} is generated so that it fits the actual ratio R^{SEN} measured by MERIS. CWV values are changed iteratively to seek for the value making R^{SIM} to fit R^{SEN}. The Merit Function χ(CWV) to be minimized for this inversion is

$$\chi(CWV) = R^{SEN} - R^{SIM}(CWV). \quad (2)$$

The function χ may have either positive or negative values. Then, the minimization of χ(CWV) consists in finding the root of a 1-D function.

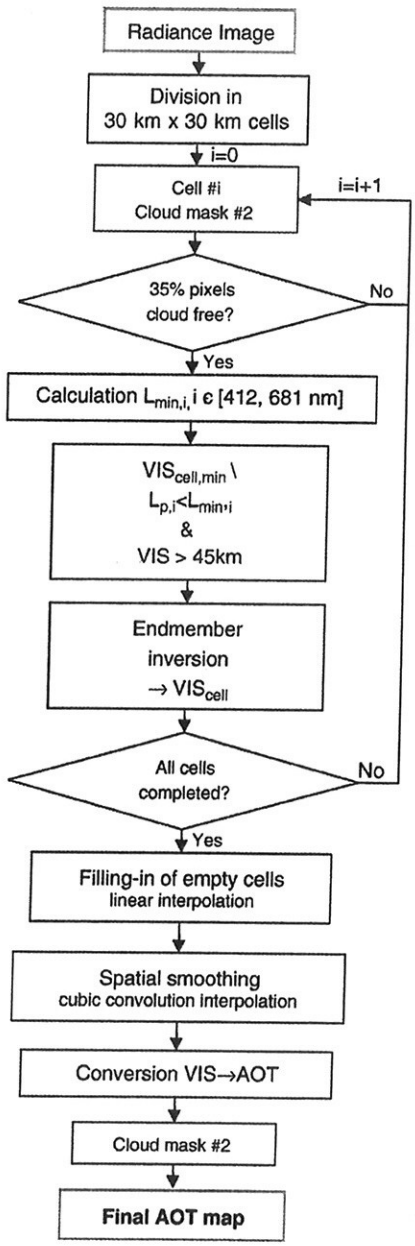

Fig. 6. Flow chart describing the main steps for AOT retrieval.

This enables the application of the fast Brent's method (Press et al., 1986) to estimate the water vapor content with a low time penalty.

Given the angular configuration, the AOT and the surface elevation and slope for each pixel, the surface reflectance at bands 14 and 15 must be known for the simulation of R^{SIM}. However, surface reflectance cannot be estimated until information about the CWV is available. This interdependence is solved by assuming a default CWV value (2 g cm^{-2}) for the retrieval of reflectance at bands 13 and 14. The reflectance at band 15 is calculated from linear extrapolation using bands 13 and 14. The absence of absorptions in the surface constituents and the linear spectral response of land targets in this reduced spectral range between 865 and 900 nm are assumed to justify the extrapolation.

Although only a residual contribution of water vapor is found in MERIS band 14, it can still affect the retrieved surface reflectance used as a basis for the inversion of Eq. (2), especially in the case of high water vapor loadings. This problem is solved by an iterative procedure. The CWV value derived after the assumption of CWV=2 g cm^{-2} for the estimation of surface reflectance is used as input in a new iteration so that the CWV applied to the reflectance retrieval in bands 13 and 14 is much closer to the actual value than the default 2 g cm^{-2}.

2.6. Retrieval of surface reflectance

Once the atmospheric state has been properly characterized, the analytical inversion of Eq. (1) is used to retrieve surface reflectance from the TOA radiance image provided by the sensor in those pixels identified as land by cloud mask #2. Atmospheric parameters are calculated on a per-pixel basis so that pixel-to-pixel variations in AOT, CWV, and surface elevation and topography are properly taken into account.

TOA radiance images are corrected from atmospheric effects in 12 of the 15 MERIS bands in this way. The bands treated from a different approach are 2, 11 and 15. On one hand, a calibration problem in MERIS band 2 (centered at 442.5 nm) may explain a spike in reflectance spectra which usually appears after atmospheric correction. Since no absorption feature is located around 442.5 nm, this might be caused by problems in the corresponding gain coefficient, which might be optimized for the medium reflectance levels in water bodies, that are brighter than most of land surfaces at the blue spectral region. No reported information has been found about this issue. On the other hand, bands 11 and 15 are affected by oxygen and water vapor absorptions. If those two bands are processed following the same scheme as the others, errors in reflectance are likely to appear due to either slight errors in radiative transfer calculations or in the sensor spectral calibration. Therefore, with the aim of "making-up" the final reflectance spectra, reflectance at bands 2, 11 and 15 are calculated by either interpolation or extrapolation with the adjacent bands.

The final step in the atmospheric correction algorithm is the correction of errors in reflectance due to the adjacency effect. A simple formulation (Vermote et al., 1997) based on weighting the strength of the adjacency effect by the ratio of diffuse to direct ground-to-sensor transmittance is used. It is only performed over FR data, as adjacency effects are considered negligible in RR images (pixel size about 1.2 km), while they could still have some impact on MERIS FR data (pixel size about 300 m).

As last step of the SCAPE-M processing chain, the reflectance image, as well as the other atmospheric correction outputs, can be geometrically corrected. The mapproj processor, supplied with the BEAM software, can be triggered by user command in order to obtain the images geo-rectified onto the latitude/longitude projection.

3. Sensitivity analysis

The impact that different factors, such as the atmospheric state, the target elevation or the surface roughness, may have over AOT, CWV and surface reflectance retrievals was investigated by a sensitivity analysis using synthetic MERIS data sets trying to reproduce representative conditions of MERIS acquisitions. Synthetic spectra were generated using MODTRAN4 in forward mode. It is assumed that the forward model which generates TOA radiance is error-free, so that all error sources are associated to wrong input values or the performance of SCAPE-M modules. No noise has been added to the data, because of the MERIS low noise-equivalent radiance of about $1–5\cdot10^{-5}$ W/m^2/sr/μm (Rast et al., 1999). It is assumed that the impact of noise on AOT, CWV and surface reflectance retrievals is negligible with respect to other error sources.

3.1. Sensitivity of AOT retrieval

The performance of the AOT retrieval method is tested in the first place. The VZA was set to 20°, SZA to 28°, RAA to 150° (measured from North to East), the surface was tilted 10° towards the sun and was located 300 m above the sea level. The water vapor column content was 2 g cm^{-2}. The surface reflectance was generated by linear combinations of green vegetation and bare soil endmembers, which were grouped in sets of 5 spectra to simulate the 5 reference pixels. Twelve different green vegetation spectra were combined to check the sensitivity of the AOT retrieval module to the target spectral response. In each of the 5 spectral clusters, the abundances for the vegetation endmember were taken from a typical case of {0.9, 0.8, 0.65, 0.6, 0.2}, while abundances for bare soils were set to one minus the vegetation abundance. The atmospheric turbidity was varied from hazy to clear, with 9 AOT values of {0.62, 0.45, 0.36, 0.31, 0.27, 0.22, 0.20, 0.16, 0.12}, corresponding to visibility values of {14, 20, 25, 30, 35, 40, 50, 70, 90} km. The resulting data set consists of 12×9 sets of 5 reference pixels.

The AOT retrieval module was run over the 12×9 sets of reference pixels adding uncertainties in surface elevation, surface slope and CWV, as well as varying the different surface reference spectra. It is assumed that the observation and illumination angles are known. The most important conclusions were:

- Sensitivity to target reflectance response: the AOT at 550 nm Root Mean Square Error (RMSE) for the 75% of the tested vegetation pixels was less than 0.03, the average from all of them being 0.026.
- Errors of ±300 m in the surface elevation may lead to errors up to 0.08 in AOT. However, we can discard elevation as error source because of the use of a DEM in the processing.
- Deviations of ±1 g cm^{-2} from the CWV input of 2 g cm^{-2} may lead to errors up to ±0.03 in AOT for the highest AOT values, but it is negligible for the medium and low AOT values.
- No appreciable contribution to AOT retrieval accuracy has been found from errors in the surface slope and orientation up to ±10°.

An orientative error figure for AOT retrievals was calculated by grouping errors in the input variables which led to either overestimation or underestimation in AOT retrieval. It was stated that the overall RMSE is close to 0.03, both for the positive and negative bias. This reinforces that mismatches between real vegetation patterns and the endmembers are a major error source in the AOT retrieval module, as around 70% of the total error is associated to this factor. Thus, ±0.03 can be assumed as the intrinsic error associated to AOT retrievals with the method presented in this work. It must be remarked, however, that errors due to deviations from the rural aerosol model and to mismasked cloudy pixels are not represented by that figure.

3.2. Sensitivity of CWV retrieval

An analog study was performed for CWV retrievals. The same configuration than in the case of AOT was used, except for CWV was now varied in the range of values {0.4, 0.8, 1.2, 1.6, 2.0, 2.4, 2.8, 3.2, 3.6, 4.0, 4.4} g cm^{-2}, while the AOT at 550 nm was fixed to 0.36. Surface reflectance was again given by linear combinations of vegetation and bare soil to analyze the influence of reflectance brightness and spectral slope on CWV retrievals. In addition, the impact of spectral

shifts in MERIS spectral calibration within the across-track direction was studied. The most important conclusions are:

- An average RMSE about 0.05 g cm^{-2} is calculated from all the CWV variation range if the loop to refine the 2 g cm^{-2} default value is not performed.
- Relative errors associated to surface spectral slope and topography are less than 0.5%.
- Elevation and AOT are important error sources for CWV. In particular, errors about ±0.06 g cm^{-2} appear when errors in elevation are about ±300 m, while they are about ±0.13 g cm^{-2} when the uncertainty in AOT at 550 nm is in a range of ±0.15 around the 0.36 input value.
- The most important errors are associated to spectral calibration. Depending on the pixel across track position, errors of up ±4% may be obtained for an input CWV of 2 g cm^{-2}.

For a final error figure, again all the factors leading to either underestimating or overestimating the CWV content were clustered to derive CWV from a set of TOA radiance spectra. However, it was stated that CWV errors are mainly driven by the spectral shift if values similar to those in the previous section and AOT variations of 0.03, are assumed. For this reason, an overall relative error in CWV of 4%, peak error for the reference 2 g cm^{-2} value, is chosen as representative of all CWV retrievals.

3.3. Sensitivity of reflectance retrieval

For the analysis of the accuracy in surface reflectance retrieval, the spectra derived from the atmospheric correction of the synthetic data base are compared to those used as inputs. Again, surface elevation, topography effects and uncertainties in AOT and CWV were added to SCAPE-M. It is concluded that:

- AOT influence is higher in the shortest wavelengths, due to the spectral dependence of aerosol scattering. Errors up to ±100% in dark vegetation reflectance were estimated at those wavelengths. Moreover, errors in reflectance due to bad estimations of the aerosol content are also meaningful inside gaseous absorptions at MERIS bands 11 (oxygen) and 15 (water vapor), due to the different impact of multiple scattering inside and outside absorption bands.
- Errors in CWV are only noticeable in band 15, what justifies the separation of reflectance and CWV retrievals in MERIS algorithms.
- Errors in reflectance due to a bad estimation of surface elevation can be up to ±30% in the blue wavelengths for low reflectance targets due to Rayleigh scattering contribution.
- Surface slope and orientation affect reflectance retrievals considerably in the whole spectrum, with errors between ±10% and ±15% even in the high reflectance levels at the NIR wavelengths when errors of ±10° are added.

From all those considerations, a spectrally-constant error of ±8% is assumed for reflectance retrievals in SCAPE-M.

4. Results

4.1. Validation methodology

Different data sources have been employed in the validation of SCAPE-M results. For the atmospheric products, AERONET sunphotometer measurements distributed all over the world have been a key tool in the assessment of the method performance under different environments and atmospheric conditions. AERONET is an optical ground-based aerosol monitoring network consisting in more than 500 stations located all over the world. These provide globally distributed near real time observations of aerosol spectral optical thickness, aerosol size distributions, and precipitable water in diverse aerosol regimes. The robustness of SCAPE-M atmospheric products against different surface and/or atmospheric conditions is assessed by comparing MERIS retrievals with concurrent AERONET data from different stations. With this purpose, more than 200 RR and 20 FR MERIS images acquired in 2003 have been processed.

The validation of surface reflectance images, in turn, is conditioned by the availability of reliable ground truth. In the case of MERIS, the spatial resolution of 300 m or 1200 m causes the direct comparison with *in situ* reflectance measurements to be hardly representative over land targets. This issue can be partially solved by using reference data with a coarser spatial resolution than ground-based measurements. For this reason, reflectance derived from a MERIS FR image acquired over the Barrax study site (La Mancha, Spain, 39.05°N, 2.09°W) on 14 July 2003 during the SPectra bARrax Campaign (SPARC) (Moreno et al., 2004) has been compared to a reflectance map derived from Compact High Resolution Imaging Spectrometer (CHRIS) on board the PRoject for On-Board Autonomy (PROBA) data acquired on the same date. The coupled CHRIS-PROBA system (Barnsley et al., 2004), provides high spatial resolution hyperspectral/multiangular data. CHRIS measures over the VNIR bands from 400 nm to 1050 nm, with 62 spectral bands at a spatial resolution of 34 m for the operation Mode-1, and an approximate swath of 15 km. CHRIS-PROBA data were processed following the procedure described in Guanter et al. (2005). The reflectance data from the CHRIS-PROBA image were validated by cross-checking against *in situ* measurements carried out by an Analytical Spectral Devices (ASD) FieldSpec Pro FR Spectroradiometer (footprint around 0.8 m, 2 nm of spectral resolution) simultaneously to CHRIS acquisitions. In addition, direct comparison of MERIS-derived reflectance data with ground-based reflectance measurements was carried out for inland water bodies, where a larger homogeneity in spectral reflectance response is expected.

On the other hand, SCAPE-M products have been compared with equivalent MERIS-based products, such as the MERIS L2 CWV product (Bennartz & Fischer, 2001) and AOT and reflectance maps generated by the BAER method (von Hoyningen-Huene et al., 2003). The MERIS L2 AOT product (Santer et al., 1999) was not used because only a small amount of pixels with a successful AOT retrieval was found in the L2 images available for this work.

4.2. Results from AOT retrieval

SCAPE-M-derived AOT from all the non-cloudy points with a temporal separation between MERIS and AERONET acquisitions lower than ±1 h are plotted in Fig. 7. It must be remarked that the scatter plots are automatically generated by a routine reading from AERONET files and MERIS images and finding concurrent points, and that only the points classified as cloudy have been removed. No other criterion for the discrimination of potential outliers has been applied, with the aim of being realistic in the analysis of the method potential and limitations. The RMSE in the plots is calculated according to the standard definition.

The first conclusion from Fig. 7 is that the aerosol loading is well retrieved in the general case, as it is confirmed by the high linear correlation found from the comparison with most of AERONET sites. In absolute terms, the comparison depends on the total aerosol loading, as high correlations are found for low aerosol regimes, whereas some systematic underestimation is detected as AOT increases. A different modeling of the AOT variable in the different RTCs used in the inversion of radiance measurements, both in SCAPE-M and AERONET, is considered as a possible explanation for these deviations at the largest aerosol regimes. This trend is represented by slopes in regression lines smaller than one, mostly caused by AOT at 550 nm values larger than 0.4. In particular, slopes about 0.8 and square Pearson's correlation coefficient R^2 about 0.73 are obtained from the Avignon, Carpentras and Palencia stations. Correlation slopes are smaller in the Evora and Toulouse sites (0.703 and 0.597, respectively), leading to a larger underestimation of AOT at 550 nm at the largest values. However, the high linearity in the comparison still holds (R^2=0.817 in Evora, R^2=0.728 in Toulouse). Typical RMSEs are about 0.05, which is in agreement with the 0.03 estimated as the intrinsic uncertainty associated to the method. It can be checked that

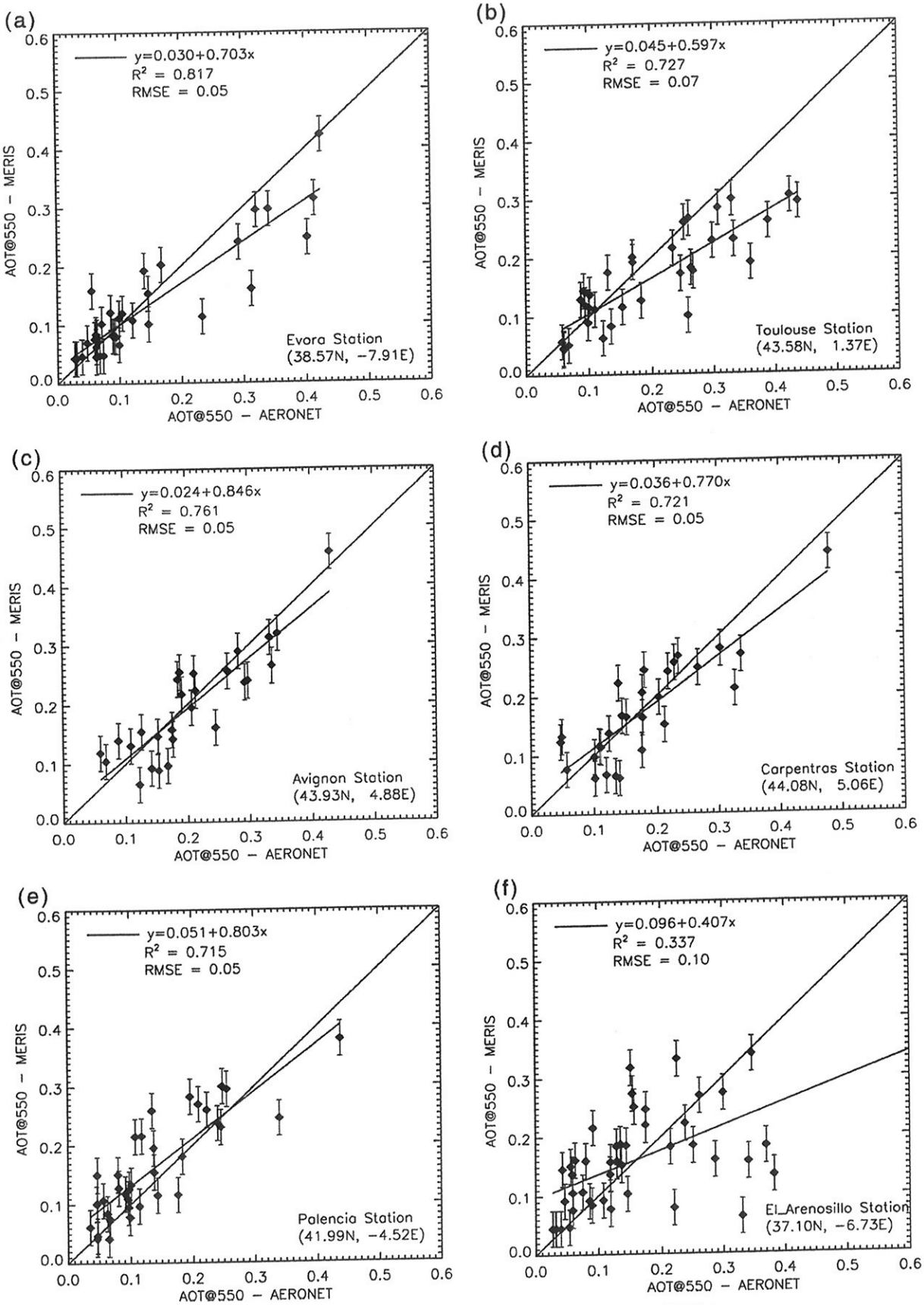

Fig. 7. Comparison of SCAPE-M-derived estimates of AOT at 550 nm with AERONET data.

those values are comparable to those calculated from MODIS (Remer et al., 2005) and AATSR data (Grey et al., 2006b), despite the fact that MODIS and AATSR are more suitable than MERIS for aerosol remote sensing because of the 2100 nm channel and the dual-view capability, respectively. Spatial coverage of aerosol maps is also improved with respect to equivalent MERIS products.

The worst situation comes from the comparison with the El Arenosillo site, where no linear correlation with MERIS retrievals is found (R^2=0.337, slope of 0.407, leading to a RMSE of 0.10).The most probable reason to explain such bad results in the El Arenosillo site is the particular environment in which the station is located. El Arenosillo is in the South of the Iberian Peninsula, nearly in the Atlantic shore and less than 200 km from Northern Africa. Thus, it is strongly influenced by maritime or Saharan aerosols, which are not well parameterized by the rural aerosol model. This may lead to a bad characterization of the aerosol properties, which would vary with wavelength. This trend has been confirmed by comparing MERIS retrievals at 440 and 870 nm reference wavelengths with AERONET data from the El Arenosillo station. A noticeable dependence of the correlation with the observation channel is found, changing from 0.41 at 440 nm to 0.156 at 870 nm. On the other hand, severe calibration problems in the Cimel instruments operating at El Arenosillo site in 2000–2001 have been reported (Cachorro et al., 2004). No information about the calibration and processing algorithms of the El Arenosillo station on 2003 is available, so errors that are intrinsic to the data acquisition and processing cannot be discarded either.

The improvements associated to MERIS finest spatial resolution of 300 m were also probed. Seventeen MERIS FR images acquired from February to November 2003 over Toulouse were processed and validated against AERONET measurements. A good discrimination between clear and turbid atmospheric conditions was stated. It was observed that the linear correlation increases with respect to the RR case, with R^2 up to 0.925. The mean value of the slope also grows from 0.6 to about 0.7. These improvements are mostly due to the increase in spectral contrast (purer pixels can be selected as reference pixels for the aerosol retrieval) associated to the finer spatial resolution of FR images.

A special atmospheric situation was present during the forest fires episodes in Portugal on August 2003, which destroyed more than 50,000 ha of forest and bushes in the first weeks of August. The magnitude and temporal persistence of Portugal fires on 2003 enable they can be monitored from MERIS data, as it was reported in von Hoyningen-Huene et al. (2005). The high aerosol loading associated to Portugal fires can be quantified by checking the Evora AERONET station archive. AOT at 550 nm derived from a series of MERIS images is compared with AERONET data for the time period between July and December 2003 (data from January to June were not available) in Fig. 8. MERIS data come from a series of 133 MERIS RR images acquired over the Iberian Peninsula from January to December 2003. After cloud screening, 35 dates of concurrent MERIS and AERONET data are available. As it can be stated in Fig. 8, both AERONET and MERIS detect the highest aerosol loadings for the day-of-year (DOY) range from 211 to 242 corresponding to August. A general good agreement between MERIS and AERONET AOT at 550 nm values, both in absolute terms and in the temporal evolution, is found all over the time period.

It must be remarked that previous experiences in AOT retrieval from other sensors suggest that the accuracy of AOT retrievals can be strongly conditioned by the scattering angle subtended by sun, target and sensor (Chylek et al., 2005). However, no analysis of this dependency for MERIS data is performed in this work. This is justified by MERIS FOV of 68.5°, which makes that VZAs higher than 30° are hardly found. This near-nadir observation is assumed to minimize changes in AOT retrieval with the scattering angle.

4.3. Results from CWV retrieval

The intercomparison between the CWV derived from MERIS RR with that from the AERONET data is resumed in Fig. 9. Vertical error bars

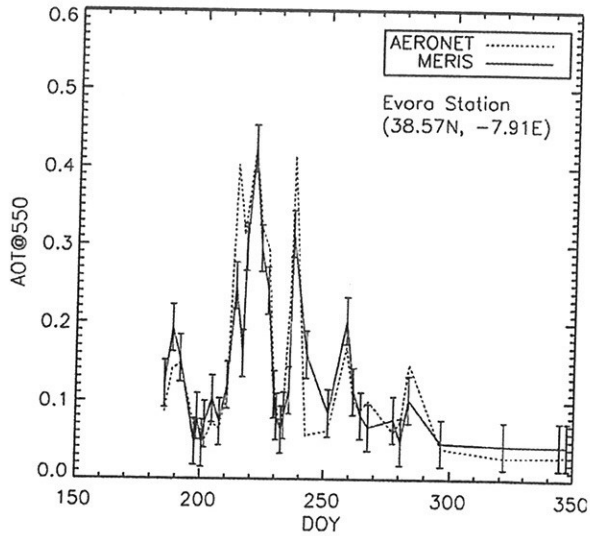

Fig. 8. Comparison of AOT at 550 nm time series for the Evora site between July and December 2003 derived from both MERIS and AERONET data. Vertical error bars correspond to the ±0.03 error in AOT at 550 nm estimated for SCAPE-M retrievals.

account for the 4% associated to CWV retrievals after the sensitivity analysis. A good correlation between MERIS and AERONET data is found in general, with slopes and R^2 close to 1 and RMSE around 0.2 g cm^{-2}, although a small overestimation of 0.1–0.2 g cm^{-2} is detected in most of the cases. However, the goodness of the comparison shows to be dependent on the AERONET site, as either relatively good or bad correlations are obtained in certain sites without a clear justification. In fact, the two extreme cases are Avignon and Carpentras, which are spatially separated by only tens of kilometers. In the first station, CWV retrieved from MERIS images matches very well AERONET measurements, with R^2=0.973, slope of 0.955 and RMSE of 0.14 g cm^{-2} being calculated by a linear regression. However, these values are very different when MERIS results are compared with the data from the Carpentras station, where the regression results are R^2=0.746, slope of 0.754 and RMSE of 0.38 g cm^{-2}. It is difficult to associate that bad comparison in Carpentras to the CWV retrieval technique, as there is not any a priori assumption on the target nature, as long as it is a land surface (not cloud or water body). I.e., there is not any reason to predict that the method will work well in Avignon and not in Carpentras. Thus, errors calculated from the comparison with the Carpentras station could be somehow related to the Carpentras station itself and the processing technique leading to the precipitable water vapor product, which are unknown. Moreover, the AOT at 550 nm derived from MERIS data over Carpentras was well correlated with the station measurements (Fig. 7 (d)), what leads to discard radiometric problems to a large extent. The same can be applied on the other way round: very poor correlations were obtained from the comparison of MERIS-derived AOT at 550 nm with the data available in El Arenosillo station, while CWV retrievals from the same sources are highly correlated (R^2=0.976, slope of 0.948 and RMSE of 0.18 g cm^{-2}). The applicability of the method to high CWV contents was also checked by comparing MERIS retrievals with ground-based measurements in the Amazon jungle. The high water vapor contents of 4 g cm^{-2} on average were well retrieved by SCAPE-M (R^2=0.956, slope of 1.11 and RMSE of 0.22 g cm^{-2}). It must be reminded that 5 g cm^{-2} is the maximum CWV tabulated in the LUT, so SCAPE-M cannot deal with higher values.

Further analysis making use of the same MERIS RR data set is performed by plotting SCAPE-M retrievals against the MERIS ESA L2 CWV product, which has been independently validated (Ciotti et al., 2003; Li et al., 2003). A scatter plot comparing ESA L2 CWV product with SCAPE-M retrievals in a 400×400 pixels window from a MERIS RR image acquired on 13 June 2003 over Southern Europe is depicted

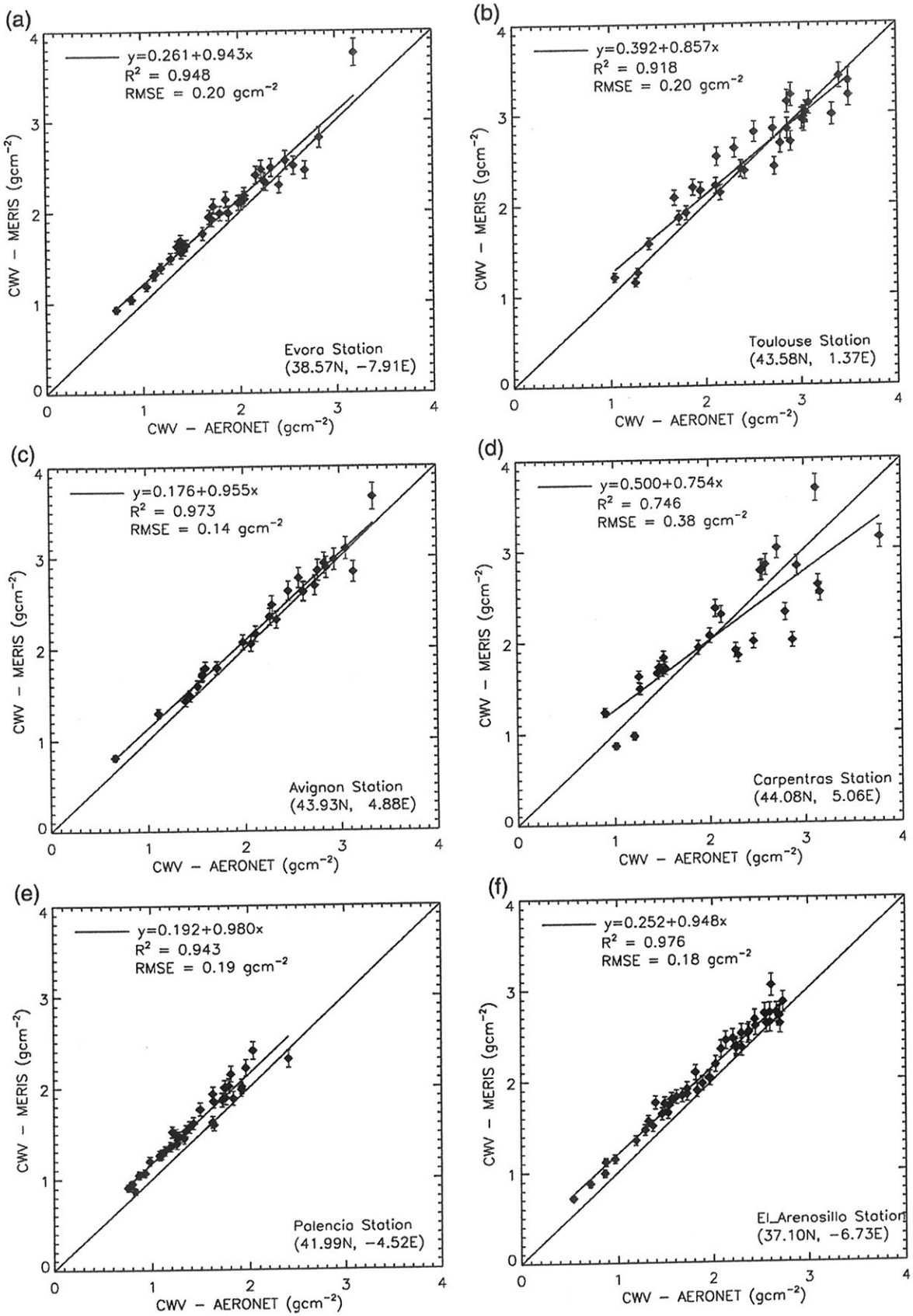

Fig. 9. Comparison of SCAPE-M-derived CWV with AERONET data.

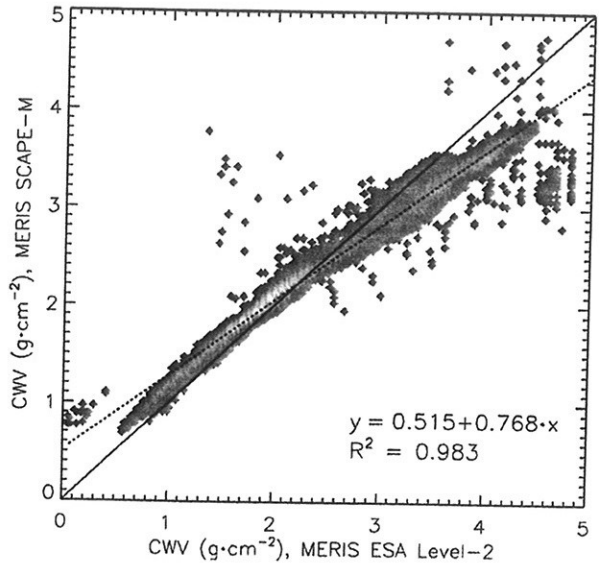

Fig. 10. Comparison of ESA Level-2 and SCAPE-M CWV retrievals in a 400×400 pixels window from a MERIS RR image acquired on 13 June 2003 over Southern Europe.

in Fig. 10. A general good correlation between the two products was found, with R^2 about 0.98, although the typical slope and bias figures deviate more from 1 and 0, respectively, than in the comparison between SCAPE-M and AERONET water vapor data. Similar comparisons were carried using other subsets from different MERIS images. Subsets were selected so that a variety of water vapor amounts, from dry to wet conditions, and topographic conditions, with flat or rough terrain at different elevation ASL, are considered. It was stated that both the mean CWV in the area and the surface elevation have an impact on the correlation between the two methods, but it has not been possible to derive a universal functional dependence from all the analyzed subsets. The general rule is that SCAPE-M overestimates with respect to the ESA product when the surface elevation is medium-high (about 300–400 m ASL), while this tendency is reversed for lower elevations. In any case, if the detected underestimation of SCAPE-M respecting to the ESA product for the lowest elevation targets holds, a better comparison between SCAPE-M and AERONET products than between ESA and AERONET could be predicted: the positive bias found in SCAPE-M CWV retrievals when compared with AERONET would be increased for the ESA L2 product, as 5 of the 6 stations in Fig. 9 are below 300 m ASL.

Sample maps of AOT at 550 nm and CWV derived by SCAPE-M from MERIS RR data acquired over the Iberian Peninsula are shown in Fig. 11. The good sampling of SCAPE-M retrievals even in semi-arid conditions as those in Southern Spain can be stated. The successful separation of different atmospheric conditions, either clear and turbid or dry and humid, can be also observed in the maps in Fig. 11.

4.4. Results from surface reflectance retrieval

Reflectance data generated from CHRIS-PROBA and MERIS images acquired simultaneously during the SPARC campaign in Barrax are used for the validation of surface reflectance retrieval over land. Some reflectance spectra were manually extracted from the CHRIS-PROBA image to compare with MERIS-derived reflectance spectra in Fig. 12. A more systematic analysis based on the degradation of the CHRIS-PROBA image up to 300 m per pixel and the co-registration with the MERIS image was considered at first, but it was discarded afterwards because errors in resampling and geometric correction were not negligible against those associated to the atmospheric correction itself. View angles are close to nadir observation for both MERIS and CHRIS. Representative targets of vegetation and bare soil pixels have been chosen. The purest pixels have been selected in the case of MERIS. CHRIS spectra are calculated as the mean value of all the pixels inside a 300×300 m window simulating a MERIS FR pixel, and the error bars correspond to the standard deviation in that window. The error bars around MERIS spectra come from the 8% relative error in reflectance which was estimated in the sensitivity analysis for SCAPE-M retrievals. Despite the very different spatial resolution in both sensors, a good matching between MERIS and CHRIS surface reflectance spectra is found for a variety of land targets. It can be noted that pure green vegetation pixels can still be found despite the 300 m resolution in MERIS, thanks to the size and homogeneity of Barrax crops. It is confirmed that MERIS spectra are mostly within the reflectance range marked by the error bars in the CHRIS spectra. It must also be remarked that worse correlations

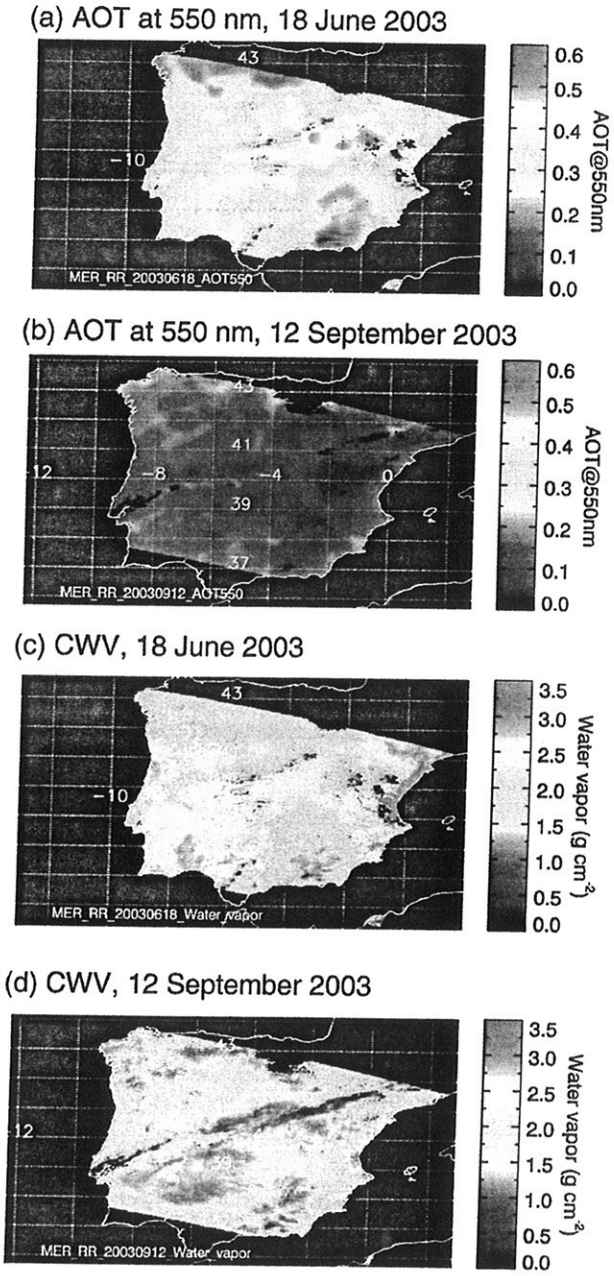

Fig. 11. AOT at 550 nm and CWV over the Iberian Peninsula derived by SCAPE-M from MERIS RR data.

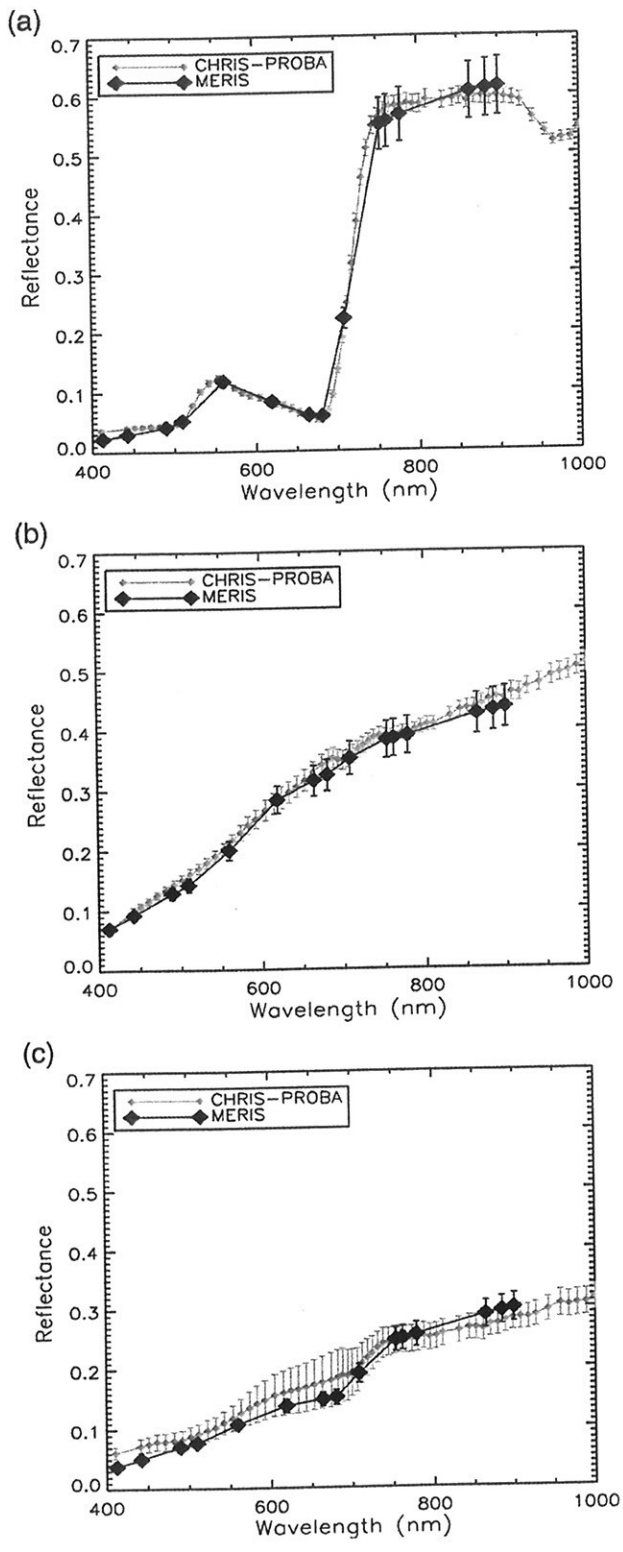

Fig. 12. Comparison of CHRIS-PROBA and MERIS derived surface reflectance spectra.

would be found in some other targets, which are assumed to be strongly driven by the surface heterogeneity. In any case, the existence of pixels where a high correlation is found supports SCAPE-M retrievals.

SCAPE-M-derived surface reflectance maps have also been compared to the equivalent product generated by the BAER method. The

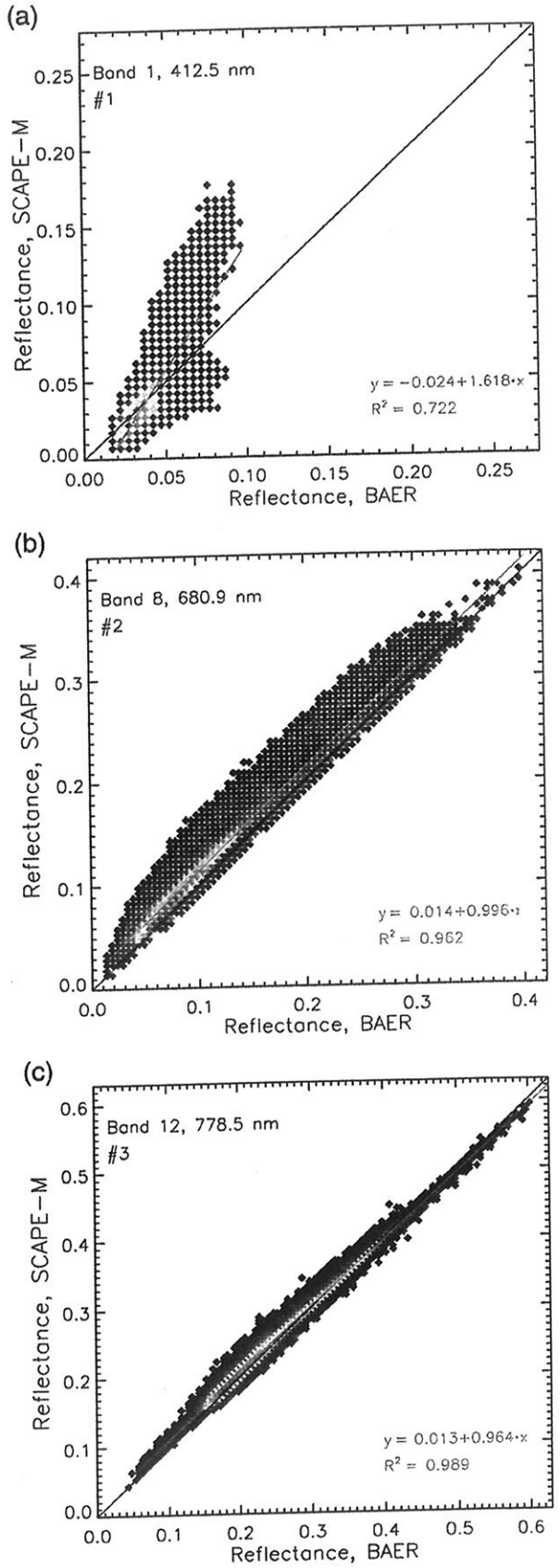

Fig. 13. Comparison of the BAER surface reflectance product and SCAPE-M retrievals, for a sample 400×400 pixels area and three MERIS bands.

surface reflectance map derived by the BAER algorithm after processing a MERIS FR image acquired over Barrax on 14 July 2003 is compared to the equivalent map as derived by SCAPE-M. It was observed that the proportion of pixels where the correction failed is much larger in the case of BAER. Typical percentages of proportion of processed pixels over the Iberian Peninsula are about 45–55% for BAER, and about 85–95% for SCAPE-M. This is due to BAER only calculates surface reflectance in those pixels in which a successful aerosol retrieval was achieved. Since AOT estimation is only performed over those surfaces where a certain proportion of green vegetation is detected, large areas in the image, mostly consisting of dry bare soils and senescent vegetation, are not processed. The interpolation and smoothing of the atmospheric retrievals which is carried out by the SCAPE-M method enables to obtain continuous surface reflectance image, with only cloudy pixels and water bodies being masked out.

Surface reflectance values retrieved by SCAPE-M and BAER were also compared for quantitative analysis. Scatter plots for three spectral channels (412.5, 680.9 and 778.5 nm) and an area of 400×400 pixels are presented in Fig. 13. Equivalent plots were generated from other 400×400 pixels windows. Only those pixels where both BAER and SCAPE-M provided a surface reflectance value are plotted. The scatter plots are built by classifying all the reflectance values into 0.005-width bins. Colors range from blue for the less populated categories to the red for the ones with the highest number of occurrences. It can be stated that the comparison is strongly influenced by the spectral band, but similar trends are observed in all the investigated 400×400 pixels windows. Low correlations are found in the blue channel, while they become higher as wavelength is increased. In the case of band 1, the categories with the largest number of pixels are located close to the 1:1 line, although there is a high proportion of categories showing a low correlation. This leads to R^2 being of the order of 0.7, with slopes higher than 1.5 and negative biases. The low reflectance values around 0.03 are caused by the fact that AOT retrievals in BAER are only performed over vegetated areas, whose reflectance in the visible wavelengths is very low. In the case of the red band centered around 681 nm, the linear correlation is very high, with R^2 higher than 0.97, slopes around 1 and small positive biases around 0.01. The mean reflectance value is around 0.1, which is also characteristic of pixels with a major contribution of green vegetation. Those results improve slightly in band 12, as the R^2 coefficient and the slope of the fit are again close to 1, but the bias around 0.01 is relatively smaller than in the red band due to the larger reflectance values. This dependence on the wavelength may be explained by the impact of residual errors in the atmospheric correction in dark targets: a bad characterization of the atmospheric state, which can be associated to errors in aerosol or water vapor retrieval, to neglecting elevation or topographic effects or even to adjacency or directional effects, may lead to noticeable errors in the subsequent surface reflectance when these ones are relatively low. Some of those factors are considered by the SCAPE-M model, but not by BAER.

A final test of SCAPE-M atmospheric correction is carried out by analyzing surface reflectance of water bodies. It was discussed in Section 2 that the retrieval of AOT is performed using land pixels as a basis, but the estimated aerosol loading in the 30×30 km^2 cells could be applied for the processing of inland and coastal waters inside those cells. The CWV is retrieved on a per-pixel basis over land surfaces, so a default value of 2 g cm^{-2} is applied over water targets. Ground-based measurements are used again for the assessment of the retrieved reflectance. Since less variability is expected in water bodies than in land surfaces, a direct comparison of *in-situ* reflectance measurements with MERIS-derived spectra is performed. A field campaign directed by the *Centro de Estudios y Experimentación de Obras Públicas* (CEDEX) on 19 June 2003 collected reflectance spectra from several reservoirs at the North–West side of the Iberian Peninsula. The comparison of MERIS-derived reflectance spectra with ground-based measurements over the Tremp ("TR", 42.19N, 0.93E), Terradets ("TD", 40.07N, 0.89E), Rialb ("RL", 41.96N, 1.20E) and Caselles ("CA", 42.00N, 0.62E) reservoirs is displayed in Fig. 14. A general good correlation is found from the comparison, despite the different spatial and temporal resolution of the two data sources: MERIS-derived spectra are extracted from the center of the reservoir and not from the exact position where the ground measurement was taken, in order to minimize a potential contribution to reflectance from land surfaces in the surroundings. Moreover, MERIS acquisition was at 10:20 a.m., while field measurements were taken in a wide time range from 8:55 a.m. to 4:10 p.m. In any case, both the spectral shape and the average brightness indicate SCAPE-M retrievals over inland waters may be reliable enough for the application of algorithms for the retrieval of water features from satellite data.

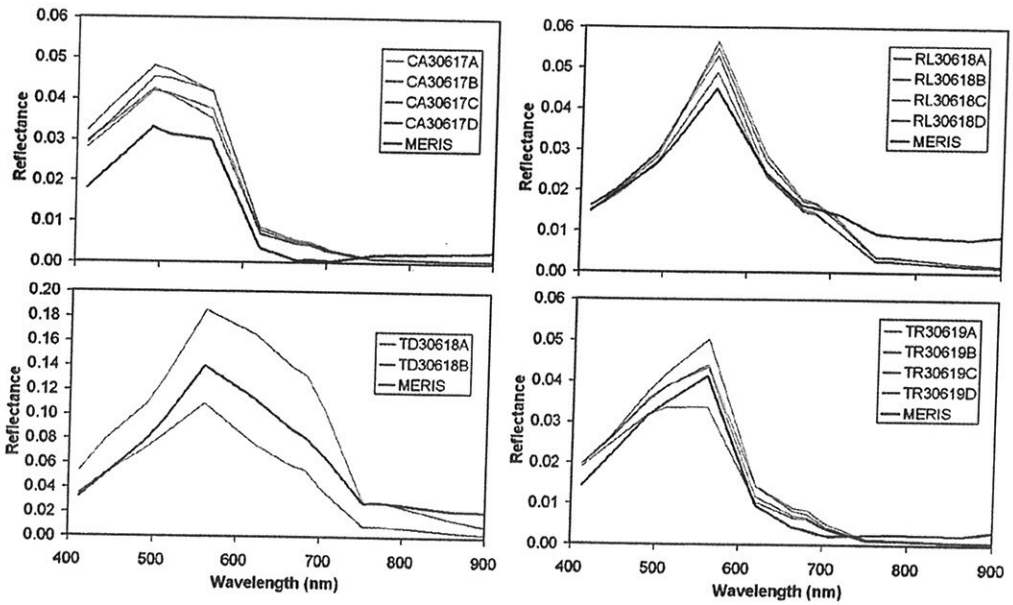

Fig. 14. Comparison of MERIS-derived water reflectance spectra with ground-based measurements over North–West Iberian Peninsula on 19 June 2003.

5. Summary and conclusions

The SCAPE-M method for the atmospheric processing of ENVISAT/MERIS L1b data has been presented in this paper. It is intended to derive AOT, CWV and reflectance maps from MERIS data over land in a consistent and automatic manner. The fundamental basis of SCAPE-M has been reported in the first place by describing the different modules used in the processing. Secondly, a sensitivity analysis to estimate method performance is presented. A number of input combinations and atmospheric situations representing MERIS real acquisitions have been simulated. It has been found that the most important dependence on AOT retrieval is the particular spectral pattern of the reference pixels used for the inversion. CWV is mostly affected by MERIS spectral calibration, through spectral shifts from the band setting at which the LUT is generated. Overall errors in AOT of ±0.03 and ±4% in CWV have been estimated. For surface reflectance, a mean relative error of ±8% is associated in the whole 400–900 nm range. Further information on SCAPE-M performance is obtained by an extensive validation exercise including both atmospheric and reflectance products.

Many statements and conclusions have been highlighted within the different topics addressed along this work. Some of them can be outlined here as the main concluding remarks.

- The retrieval of AOT over land is a complex task. Some points remain open to further investigation:
  - A proper estimation of the aerosol model is a challenging topic, especially in the case of MERIS (400–900 nm and one single view angle). The inclusion of parameters describing the aerosol model adds extra free parameters to the inversion of TOA radiance, and MERIS spectral/angular configuration seems not sufficient to achieve robust values for all the parameters. For this reason, the rural aerosol model was adopted for the generation of the LUT. However, this may lead to inaccurate AOT retrievals when other aerosol types are present.
  - The spatial variation of aerosols must be investigated. The method proposed in this work performs AOT retrievals based on 30×30 km cells, in which the atmospheric state is assumed to be laterally homogeneous. This strategy provides important advantages, such as the availability of a whole area from which reference pixels can be selected and the reduction of the computational burden. However, no finer information about the aerosol distribution is obtained. This means that pixel-to-pixel variations within the cell are not detected. This would be specially relevant in topographically complex areas.
  - Unmasked cloudy pixels lead to out-of-range AOT values. This may be an important problem in the case of thin cirrus clouds, which are very difficult to detect. Some effort on developing robust cloud-masking techniques applicable to MERIS data would lead to better AOT estimations.
- The retrieval of CWV does not require such an important modeling effort. The main constraint has been found to be in the associated computational time, as retrievals on a per-pixel basis may be very time consuming for the largest images. The main error source in the case of MERIS is the variation of the band spectral positions in the along track direction of the MERIS cameras, which result in errors up to 0.2 g cm^{-2} in camera transitions.
- Apart from AOT and CWV, other factors must be considered in the retrieval of surface reflectance. It is affected by both surface elevation and topographic effects, which are normally neglected in atmospheric correction methods. SCAPE-M takes them into account. The adjacency effect is also included by a simple model, but directional effects are not considered. No adequate modeling of the surface directional reflectance has been found which could be plugged into an operational procedure. Therefore, errors associated to the Lambertian approach are assumed to be intrinsic to the method.

The validation exercise for SCAPE-M has relied on the comparison with external reference data, like AERONET stations all over the world, comparison with other satellite products and ground-based reflectance measurements.

A quantitative validation comparing SCAPE-M AOT retrievals from more than 200 MERIS images with AERONET data is carried out. Mean R^2 values were around 0.7–0.8, although some cases with very low R^2 (0.337, El Arenosillo station) or very high (0.925, Toulouse, FR data) are also found. A systematic underestimation of MERIS-derived AOT with respect to AERONET measurements for the highest aerosol loadings must be investigated.

A similar analysis is done for CWV retrievals. AERONET data were used again in order to have more spatial and temporal sampling. Very good correlations were generally found, with $R^2>0.9$ in most of the cases. Those include stations located around the Amazon jungle, where high water vapor concentrations were measured (up to 4.8 g cm^{-2}). The final study was based on comparing the SCAPE-M retrievals with the ESA official Level 2 water vapor product. Even though a general agreement was found, some deviations mainly associated to elevation was detected. In particular, SCAPE-M gave higher CWV than the ESA product for mean/high elevations (around 300 m or higher), while it happened on the contrary for targets at sea level.

Finally, surface reflectance retrievals were compared with different sources. The first one was a CHRIS/PROBA image acquired over the Barrax site at the same time than a MERIS image. The 34 m per pixel CHRIS spatial resolution enabled comparison with ground measurements, so it was used as an intermediate step between MERIS and ground-based reflectance measurements. Good correspondence in the derived reflectance patterns was found in homogeneous targets. On the other hand, SCAPE-M reflectance retrievals are also compared with BAER-derived reflectance maps. The correlation between the two products improved with wavelength, and R^2 higher than 0.96 were calculated at the red and NIR wavelengths. These values were considerably lower (around 0.7) in the case of the first MERIS band, possibly due to the high contamination by aerosols. The proportion of processed pixels over the Iberian Peninsula for SCAPE-M was higher than for BAER (typical values were about 45–55% for BAER and 85–95% for SCAPE-M). Finally, MERIS-derived water reflectance from inland water bodies were compared with concurrent ground-based measurements. A good correspondence in both the average reflectance levels and the spectral shapes was found.

Acknowledgment

This work has been done in the frame of ESRIN/Contract No 16545/02/I-LG (*Development of algorithms for the exploitation of MERIS data over land* project). LG acknowledges the support by a PhD fellowship from the Spanish Ministry of Education and Science. The authors also want to thank the Personal Investigators of all the AERONET stations providing data for this work, to R. Peña, J.A. Domínguez and A. Ruiz from CEDEX (Spain) for the reflectance measurements over inland waters, and to Rudolf Richter from DLR-DFD and three anonymous reviewers for their valuable comments. The authors would also like to devote this work to the memory of Prof. Mike Barnsley (1960-2007) for his important contribution to remote sensing and to the CHRIS-PROBA mission in particular.

References

Amans, V., & Laur, H. (2007). *Access to ENVISAT data. EOEP-GSOP-EOPG-TN-06-0001, ESA–ESRIN.*

Barnsley, M. J., Settle, J. J., Cutter, M., Lobb, D., & Teston, F. (2004). The PROBA/CHRIS mission: a low-cost smallsat for hyperspectral, multi-angle, observations of the earth surface and atmosphere. *IEEE Transactions on Geoscience and Remote Sensing, 42*, 1512–1520.

Béal, D., Baret, F., Bacour, C., & Gu, X. -F. (2007). A method for aerosol correction from the spectral variation in the visible and near infrared: Application to the MERIS sensor. *International Journal of Remote Sensing, 28*, 761–779.

Bennartz, R., & Fischer, J. (2001). Retrieval of columnar water vapour over land from backscattered solar radiation using the Medium Resolution Imaging Spectrometer. *Remote Sensing of Environment, 78*, 274–283.

Berk, A., Anderson, G.P., Acharya, P.K., Hoke, M.L., Chetwynd, J.H., Bernstein, L.S., et al., 2003. MODTRAN4 Version 3 Revision 1 User's Manual. Tech. rep., Air Force Research Laboratory, Hanscom Air Force Base, MA, USA.

Cachorro, V. E., Toledano, C., Vergaz, R., de Frutos, A. M., Sorribas, M., Vilaplana, J. M., et al. (2004). The PHOTONS-AERONET sites in Spain. Calibration problems and KCICLO correction method. *Óptica Pura y Aplicada, 37*, 3401–3406.

Chylek, P., Borel, C. C., Clodius, W., Pope, P. A., & Rodger, A. P. (2003). Satellite-based columnar water vapor retrieval with the multi-spectral thermal imager (MTI). *IEEE Transactions on Geoscience and Remote Sensing, 41*, 2767–2770.

Chylek, P., Henderson, B. G., & Lesins, G. (2005). Aerosol optical depth retrieval over the NASA Stennis Space Center: MTI, MODIS, and AERONET. *IEEE Transactions on Geoscience and Remote Sensing, 43*, 2767–2770.

Ciotti, P., Di Giampaolo, E., Basili, P., Bonafoni, S., Mattioli, V., Biondi, R., et al. (2003, July). Validation of MERIS water vapour in the central Italy by concurrent measurements of microwave radiometers and GPS receivers. *Proceedings of the IGARSS. Toulouse, France.*

Colby, J. D. (1991). Topographic normalization in rugged terrain. *Photogrammetric Engineering and Remote Sensing, 57*, 531–537.

Fomferra, N., & Brockmann, C. (2005, September). Beam — The ENVISAT MERIS and AATSR toolbox. In ESA/ESRIN (Ed.), *Proceedings of the MERIS-(A)ATSR workshop. Frascati, Italy.* http://www.brockmann-consult.de/beam/

Franklin, S., & Giles, P. (1995). Radiometric processing of aerial and satellite remote-sensing imagery. *Computers and Geosciences, 21*, 413–423.

Gómez-Chova, L., Camps-Valls, G., Calpe, J., Guanter, L., & Moreno, J. (2007). Cloud-screening algorithm for ENVISAT/MERIS multispectral images. *IEEE Transactions on Geoscience and Remote Sensing, 45*, 4105–4118.

Grey, W. M. F., North, P. R. J., & Los, S. O. (2006). Computationally efficient method for retrieving aerosol optical depth from ATSR-2 and AATSR data. *Applied Optics, 45*, 2786–2795.

Grey, W. M. F., North, P. R. J., Los, S. O., & Mitchell, R. M. (2006). Aerosol optical depth and land surface reflectance from multiangle AATSR measurements: global validation and intersensor comparisons. *IEEE Transactions on Geoscience and Remote Sensing, 44*, 2184–2197.

Guanter, L., Alonso, L., & Moreno, J. (2005). A method for the surface reflectance retrieval from PROBA/CHRIS data over land: Application to ESA SPARC campaigns. *IEEE Transactions on Geoscience and Remote Sensing, 43*, 2908–2917.

Guanter, L., González-Sampedro, M. C., & Moreno, J. (2007). A method for the atmospheric correction of ENVISAT/MERIS data over land targets. *International Journal of Remote Sensing, 28*, 709–728.

Guanter, L., Richter, R., Kaufmann, H., in press. On the application of the MODTRAN4 atmospheric radiative transfer code to optical remote sensing. International Journal of Remote Sensing.

Hay, J. E. (1979). Calculation of monthly mean solar radiation for horizontal and inclined surfaces. *Solar Energy, 23*, 301–307.

Holben, B. N., Eck, T. F., Slutsker, I., Tanre, D., Buis, J. P., Setzer, A., et al. (1998). AERONET — A federated instrument network and data archive for aerosol characterization. *Remote Sensing of Environment, 66*, 1–16.

Kaufman, Y. J., & Sendra, C. (1988). Algorithm for automatic corrections to visible and near IR satellite imagery. *International Journal of Remote Sensing, 9*, 1357–1381.

Kaufman, Y. J., Tanré, D., Remer, L. A., Vermote, E. F., Chu, A., & Holben, B. N. (1997). Operational remote sensing of tropospheric aerosol over land from EOS moderate resolution imaging spectroradiometer. *Journal of Geophysical Research, 102*, 17051–17067.

Li, Z., Muller, J. -P., Cross, P., Hewison, T., Watson, R., Fischer, J., et al. (2003, September). Validation of MERIS Near IR water vapour retrievals using MWR and GPS measurements. In ESA/ESRIN (Ed.), *Proceedings of the MERIS user workshop. Frascati, Italy.*

Moreno, J., Alonso, L., Fernández, G., Fortea, J. C., Gandía, S., Guanter, L., et al. (2005). The Spectra Barrax Campaigns (SPARC): Overview of the activities. Proceedings of the SPARC Final Workshop, ITC, Enschede, The Netherlands, 4–5 July 2005. ESA Pub. WPP-250, ESA ESTEC ISSN 1022-6656.

Nicodemus, F.E., Richmond, J.C., Hsia, J.J., Ginsberg, I.W., Limperis, T., 1977. Geometrical considerations and nomenclature for reflectance. Tech. rep., National Bureau of Standards, US Department of Commerce, Washington, DC, USA.

Press, W. H., Flannery, B. P., Teukolosky, S. A., & Vetterling, W. T. (1986). *Numerical Recipes.* Cambridge University Press.

Ramon, D., & Santer, R. (2005, September). Aerosol over land with MERIS, present and future. In ESA/ESRIN (Ed.), *Proceedings of the MERIS-(A)ATSR workshop. Frascati, Italy.*

Rast, M., Bézy, J. L., & Bruzzi, S. (1999). The ESA medium resolution imaging spectrometer MERIS – a review of the instrument and its mission. *International Journal of Remote Sensing, 20*, 1681–1702.

Remer, L. A., Kaufman, Y. J., Tanré, D., Mattoo, S., Chu, D. A., Martins, J. V., et al. (2005). The MODIS aerosol algorithm, products and validation. *Journal of Atmospheric Sciences, 62*, 947–973.

Riaño, D., Chuvieco, E., Salas, J., & Aguado, I. (2003). Assessment of different topographic corrections in Landsat-TM data for mapping vegetation types. *IEEE Transactions on Geoscience and Remote Sensing, 41*, 1056–1061.

Richter, R. (1997). Correction of atmospheric and topographic effects for high spatial resolution satellite imagery. *International Journal of Remote Sensing, 18*, 1099–1111.

Santer, R., Carrere, V., Dubuisson, P., & Roger, J. C. (1999). Atmospheric correction over land for MERIS. *International Journal of Remote Sensing, 20*, 1819–1840.

Santer, R., Vidot, J., & Aznay, O. (2005, September). Standard aerosol model families used for atmospheric correction: How comparable are they? How validate are they? In ESA/ESRIN (Ed.), *Proceedings of the MERIS-(A)ATSR workshop. Frascati, Italy.*

Santer, R., Ramon, D., Vidot, J., & Dilligeard, E. (2007). A surface reflectance model for aerosol remote sensing over land. *International Journal of Remote Sensing. 28*, 737–760.

Shettle, E.P., Fenn, R.W., 1979. Models for the aerosol lower atmosphere and the effects of humidity variations on their optical properties. Rep. tr–79–0214, U.S. Air Force Geophysics Laboratory, Hanscom Air Force Base, Massachusetts, USA.

Vermote, E. F., El-Saleous, N., Justice, C. O., Kaufman, Y. J., Privette, J. L., Remer, L., et al. (1997). Atmospheric correction of visible to middle infrared EOS-MODIS data over land surface: Background, operational algorithm and validation. *Journal of Geophysical Research, 102*, 17131–17141.

von Hoyningen-Huene, W., Freitag, M., & Burrows, J. P. (2003). Retrieval of aerosol optical thickness over land surfaces from top-of-atmosphere radiance. *Journal of Geophysical Research, 108*, 4260–4279.

von Hoyningen-Huene, W., Kokhanovsky, A. A., Burrows, J. P., Sfakianaki, M., & Kanakidou, M. (2005, September). Validation of aerosol optical thickness retrieved by BAER (Bremen AErosol Retrieval) in the Mediterranean area. In ESA/ESRIN (Ed.), *Proceedings of the MERIS-(A)ATSR workshop. Frascati, Italy.*

von Hoyningen-Huene, W., Kokhanovski, A. A., Burrows, J. P., Bruniquel-Pinel, V., Regner, P., & Baret, F. (2006). Simultaneous determination of aerosol- and surface characteristics from top-of-atmosphere reflectance using MERIS on board of ENVISAT. *Advances in Space Research, 37*, 2172–2177.